Optimization of Blade Sweep in a Transonic Axial Compressor Rotor*

Choon-Man JANG**, Ping LI*** and Kwang-Yong KIM****

This paper describes the optimization of blade sweep in a transonic axial compressor rotor. The shape optimization has been performed using response surface method and the three-dimensional Navier-Stokes analysis. Two shape variables of the rotor blade, which are used to define the rotor sweep, are introduced to increase the adiabatic efficiency of the axial compressor. Blade sweep has been used in the transonic compressor design with the intent of reducing shock losses. Throughout the optimization, optimal shape having a backward sweep is obtained. Adiabatic efficiency, which is the objective function of the present optimization, is successfully increased by 1.25 percent. Separation line due to the interference between a shock and surface boundary layer on the blade suction surface is moved downstream for the optimized blade compared to the reference one. It is noted that the increase in adiabatic efficiency for the optimized blade is caused by moving the separation line to the downstream on the blade suction surface.

Key Words: Turbomachinery, Compressor, Blade Optimization, Blade Sweep, Response Surface Method, Adiabatic Efficiency

1. Introduction

The present study is focused on the shape optimization of a transonic axial compressor rotor (NASA rotor 37). The shape optimization based on the three-dimensional flow analysis has been performed in the design process of turbomachinery blades in recent years as an efficient tool for increasing the efficiency. The flow inside a transonic axial compressor has extremely complex features due to its three-dimensional, unsteady and vortical nature[(1)-(3)]. This makes it difficult to predict accurately the compressor performance by numerical simulation. Compared to the traditional experimental techniques, computational fluid dynamics (CFD) has obvious advantages[(4)]. CFD techniques help us to analyze the effects of individual feature more easily as compared to the experimental techniques, which usually focus on the hybrid effects of several features.

Recently, the leaned, swept, and skewed blade has become a matter of interest in the design of turbomachinery blades. One of the most significant design trends is the use of aerodynamic sweep to improve the performance and stability of transonic compressor blades. An axial flow turbomachinary blade is swept when each blade section of a datum blade of the radial stacking line is displaced parallel to the relative flow direction. The pioneer study on a sweep blade for compressors has been done by Bliss[(5)]. The main objective in this study was to reduce the noise level induced by shock waves. Hah, et al.[(6)] studied both forward- and backward-swept compressor blades. They showed that a backward-swept blade can suppress the intensity of the shock loss and a forward-swept blade can suppress secondary flow and tip entropy generation. Watanabe and Zangeneh[(7)] reported that the blade sweep in the design of a transonic turbomachinery blade is an effective parameter to control the strength and position of the shock wave at the tip of the transonic rotors, and also, to control the corner separation in the stator. Denton and Xu[(8)] investigated the effects of sweep and lean on the performance of a transonic fan. They showed that the stall margin was significantly improved with the forward swept blade although a very little change in the peak efficiency was produced by the blade sweep or lean. In addi-

* Received 5th January, 2005 (No. 05-5005)
** Fire & Engineering Services Research Department, Korea Institute of Construction Technology, 2311 Daehwa-Dong, Ilsan-Gu, Goyang, Gyeonggi-Do, 411–712, Korea
*** Department of Mechanical Engineering, Inha University, 253 Yonghyun-Dong, Nam-Gu, Incheon, 402–751, Korea
**** Department of Mechanical Engineering, Inha University, 253 Yonghyun-Dong, Nam-Gu, Incheon, 402–751, Korea. E-mail: kykim@inha.ac.kr

tion, Janos Vad, et al.[9] studied experimentally as well as numerically the aspects of forward- and backward-sweep in axial flow rotors having low aspect ratio blade for incompressible flow. Their studies showed that the forward-swept bladed rotor reduces total efficiency compared to the unswept and backward-swept bladed rotors. However, the effects of sweep on transonic compressors are not fully understood yet, and further studies need to be done to have a better understanding of swept blades in transonic compressors.

Response surface method[10], as a global optimization method, is recently introduced as a tool of design optimization for turbomachinery. The response surface method smoothes out high frequency noise of the objective function, thus expected to find a solution near the global optimum. Ahn and Kim[11] used response surface method to the design optimization of axial compressor rotor blades.

In the present study, the response surface method combined with a three-dimensional Navier-Stokes solver is introduced to find optimum blade sweep in a transonic axial compressor (NASA rotor 37). A backward-swept blade is considered to enhance the adiabatic efficiency. Detailed internal flow analysis is performed in relation to the efficiency enhancement.

2. Test Axial Compressor

NASA rotor 37[12], an axial-flow compressor rotor having a low-aspect ratio, is considered for optimization in the present study. The detailed specifications of the compressor are summarized in Table 1. The rotor tip clearance is 0.356 mm (0.45 percent span). The measured choking mass flow rate is 20.93 kg/s, which corresponds to 103.67% of the design flow rate[12].

The meridional view of the axial compressor is shown in Fig. 1. Total pressure, total temperature and adiabatic efficiency in relation to the mass flow rates are measured at inlet (station 1) and outlet (station 2) positions as shown in Fig. 1[12]. The inlet and outlet positions are located at 41.9 mm upstream of the tip leading edge of the rotor and at 101.9 mm downstream of the tip trailing edge of the rotor, respectively.

Table 1 Design specifications of NASA rotor 37

Mass flow	20.19 kg/s
Rotational speed	17189 rpm
Pressure ratio	2.106
Adiabatic efficiency	0.889
Inlet hub-tip ratio	0.7
Inlet tip relative Mach no.	1.4
Inlet hub relative Mach no.	1.13
Tip solidity	1.288
Rotor aspect ratio	1.19
Number of rotor blades	36

3. Methods of Blade Optimization

3.1 Response surface method

Optimization using response surface method (RSM) is a series of statistical and mathematical processes; generation of data by numerical computations or experiments, construction of response surface by interpolating the data, and optimization of the objective function on the surface. Although RSM was devised to obtain empirical correlation from the experimental data, the ability to reduce the number of experiments let this method be applied widely to the optimization problems[13].

The polynomial-based response surfaces are commonly employed in RSM. Unknown coefficients of polynomial are obtained from a regression process. The response model is usually assumed as a second-order polynomial, which can be written as follows.

$$f = \beta_0 + \sum_{j=1}^{n} \beta_j x_j + \sum_{j=1}^{n} \beta_{jj} x_j^2 + \sum \sum_{i \neq j} \beta_{ij} x_i x_j \qquad (1)$$

where, n, β, and x_i are the number of design variables, the coefficient of variables, and selected variables, respectively. To determine the coefficients, standard least-squares regression can be used. In this case, the number of data must be larger than the number of coefficients.

In order to reduce the number of data needed for constructing a response surface and to improve the representation of the design space, the design of experiment (DOE) is important for selecting design points. Among the different types of DOE techniques, D-optimal design[14] is employed in the present work for the representation of design space. With the number of design points only 1.5 to 2.5 times the number of coefficients in the response model, reliable results can be obtained.

3.2 Objective function and design variables

In the present study, adiabatic efficiency η_{ad} is selected as an objective function of the optimization, and is defined as follows;

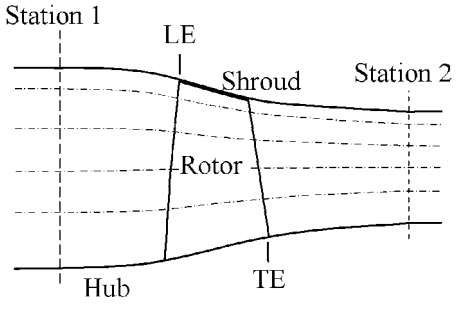

Fig. 1 Meridional view of Rotor 37

$$\eta_{ad} = \frac{(P_{0exit}/P_{0inlet})^{(\gamma-1)/\gamma} - 1}{T_{0exit}/T_{0inlet} - 1} \quad (2)$$

where, P_0 and T_0 are total pressure and total temperature, respectively.

To enhance the adiabatic efficiency of the compressor rotor, blade sweep is introduced as a variable for optimizing the blade shape. The blade sweep is defined by two shape variables, δ_1 and δ_2, as shown in Fig. 2. The variable δ_1 is defined by an axial distance from the blade leading edge of the rotor tip, and normalized by the rotor tip chord (= 56.8 mm). The variable δ_2 is defined by a distance from the hub, and normalized by the blade span of the blade leading edge (= 74.4 mm). That is, the variable δ_2 is zero at the hub, and unity at the rotor tip. It is noted that the normalized variable δ_2 defined at blade leading edge is applied to the entire blade chord including the blade trailing edge. The line between the rotor tip and the position of δ_2 is linearly connected, and the swept line between the tip and the position of δ_1 is connected according to the meridional shape of casing while the tip clearance keeps constant. The range of each variable for selection of the points for response evaluation is determined by preliminary calculations, and is summarized in Table 2.

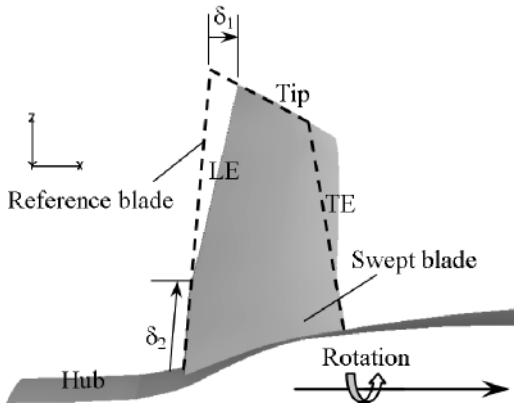

(a) Side view

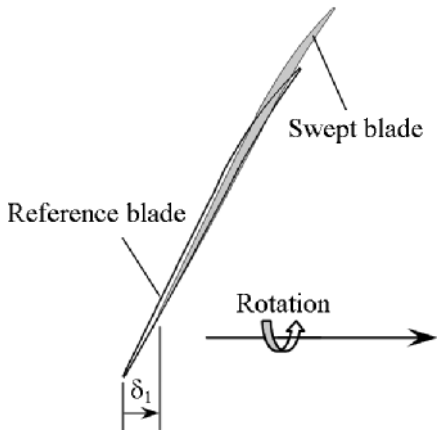

(b) Top view

Fig. 2 Definition of blade sweep

3.3 Numerical analysis method

The three-dimensional thin-layer Navier-Stokes and energy equations are solved on body-fitted grids using an explicit finite-difference scheme. An explicit Runge-Kutta scheme proposed by Jameson, et al.[15] is used to solve flow from initial to steady state with a spatially varying time step to accelerate convergence. Artificial dissipation terms have been added to resolve shocks. The algebraic turbulence model of Baldwin and Lomax[16] has been employed to estimate the eddy viscosity.

Figure 3 shows surface grids for the rotor and the hub. A composite grid system with structured H-, C-, and O-type grids is adopted to represent the complicated configuration of the axial compressor. H-type grid consists of 30×35×70 grids (in the streamwise, pitchwise and spanwise directions, respectively) and is introduced for the inlet flow region. C-type grid consists of 271×50×70 grids, and is used for the blade passage. The grid embedded in the tip clearance consists of 191×15×15 grids. The whole grid system has about 1 060 000 grid points. The average number of iterations and CPU time for the converged solution are approximately 3 000 and 3 hours with supercomputer of NEC SX-6 (144 GFLOPS), respectively

Table 2 Design space of blade sweep

Variables	Lower Bound	Middle	Upper Bound
δ_1 (%)	8.8	35.2	61.6
δ_2 (%)	0.0	22.65	45.3

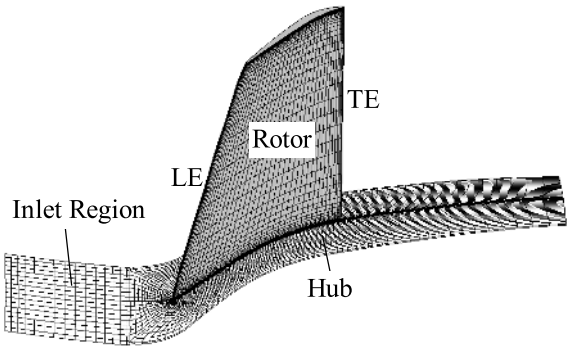

(a) Perspective view (note: every two grid lines are shown in axial and tangential direction)

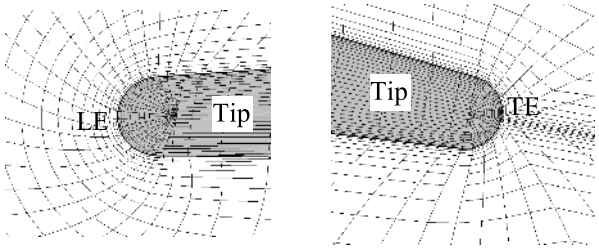

(b) View from casing at LE and TE of rotor tip

Fig. 3 Computational grids

Mach numbers in each direction, total pressure, and total temperature are given at the inlet. At exit, the hub static pressure ratio has been specified, and the radial equilibrium equation is solved along the blade span. A periodic tip clearance model is used to resolve the tip clearance flow explicitly. No-slip and adiabatic wall conditions are used at all the wall boundaries. For reducing the computational load, flow field in a single blade passage is simulated by applying periodic boundary condition in the tangential direction.

4. Results and Discussion

4.1 Validity of numerical simulation

The blade shape optimization of a transonic axial compressor rotor (NASA rotor 37) is performed using response surface method and numerical analysis. For the validation of the present numerical solutions, the spanwise distributions of total pressure, total temperature and adiabatic efficiency for the reference shape of the rotor blade are compared to the experimental results at the design flow rate in Figs. 4 – 6. In particular, the adiabatic efficiency, which is the objective function in the present study, matches well with the experimental results for the reference shape as shown in Fig. 6. However, the computational efficiency is locally overestimated compared to the experimental one near 10 and 75 percent spans. It is noted that the computational adiabatic efficiency has a maximum of 4 percent error with the experimental data at the design flow rate.

Figure 7 shows the comparison between computational and experimental distributions of adiabatic efficiency with respect to mass flow rate. In the figure, the mass flow rate is normalized with the choking flow rate (20.93 kg/s) obtained from the experiment[12]. At the design flow rate (design mass flow/ choke flow rate = 0.965 in Fig. 7), the adiabatic efficiency obtained by the numerical analysis is 1.2 percent higher than the experimental efficiency. This implies that the results of present numerical analysis are in good agreement with the experimental results.

4.2 Optimization of rotor blades

To construct a response surface for the present de-

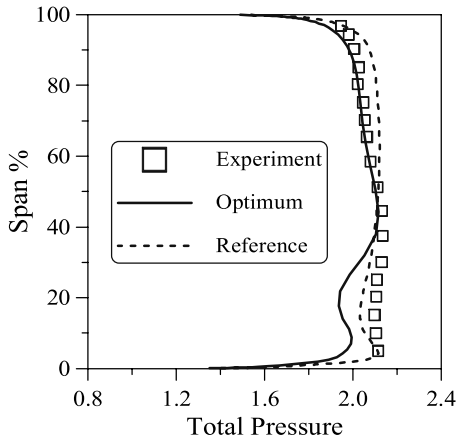

Fig. 4 Spanwise distribution of total pressure

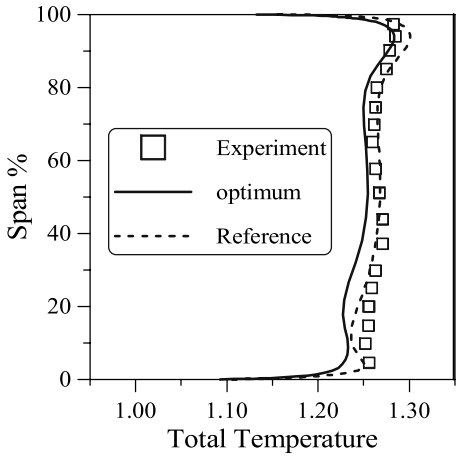

Fig. 5 Spanwise distribution of total temperature

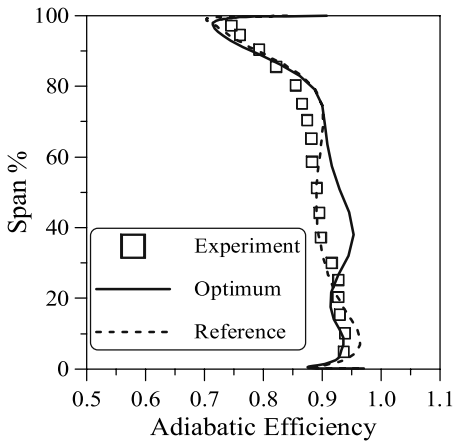

Fig. 6 Spanwise distribution of adiabatic efficiency

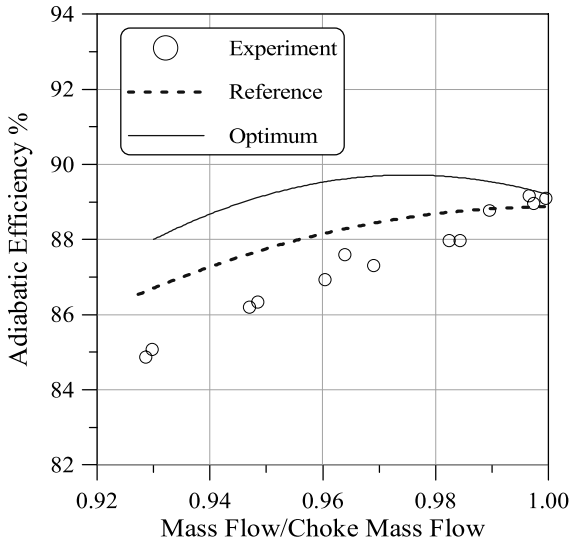

Fig. 7 Comparison of adiabatic efficiency between calculation and experiment

sign space of the blade sweep having two variables as shown in Table 2, nine training points are necessary for full factorial design. In the present study, however, seven training points are selected by D-optimal design. To measure uncertainty in the set of coefficients in a polynominal, ANOVA and regression analysis provided by *t*-statistic[17] are used and the results are shown in Table 3. Guinta[18] suggested that the typical values of adjusted R^2 are in the range, $0.9 \leq$ adjusted $R^2 \leq 1.0$, when the observed response values are accurately predicted by the response surface model. In this respect, the present response surface is reliable.

The resulting response surface is shown in Fig. 8. In this figure, horizontal and vertical axes represent the design variables of δ_1 and δ_2, respectively. The polynomial-based response surface is obtained by using a second-order polynomial as shown in Eq. (1). The optimum design variables, δ_1 and δ_2 are 19.4 percent tip chord and 13.6 percent span, respectively. It should be noted that the optimum position having maximum adiabatic efficiency is located inside the boundary of design space of the blade sweep as shown in Table 2.

Results of the blade shape optimization for a transonic axial compressor at the design flow rate are shown in Table 4. Adiabatic efficiency of the compressor, which is the objective function of the present optimization, is successfully increased by 1.25 percent. Relatively small decrease of total pressure compared to that of the total temperature is observed, thus resulting in increase of the adiabatic efficiency as defined in Eq. (2).

Figure 9 shows the three-dimensional and meridional blade shapes of the reference and the optimum rotor blades. In Fig. 9 (a), solid line represents the reference blade. It is noted that a backward-swept blade is more effective in increasing the adiabatic efficiency, which has been reported in the previous study[9].

Distributions of total pressure, total temperature and adiabatic efficiency for the reference and the optimized shapes, which are tangentially averaged at the exit of the rotor, are shown along the spanwise direction in Figs. 4 – 6. It is found in Fig. 6 that the optimum shape improves the efficiency mainly in the middle of the span, i.e., from 25 to 85 percent span. However, decreases in total pressure and total temperature are observed at almost all the span. In Fig. 7, maximum increase in efficiency is observed near the design flow rate (96.5 percent choking flow rate). From the optimization of the blade sweep in a transonic axial compressor, it is found that the blade sweep

Table 3 Results of ANOVA and regression analysis

Model	R	R^2_{adj}	Std. error of the estimate
1	0.998	0.977	0.002040933

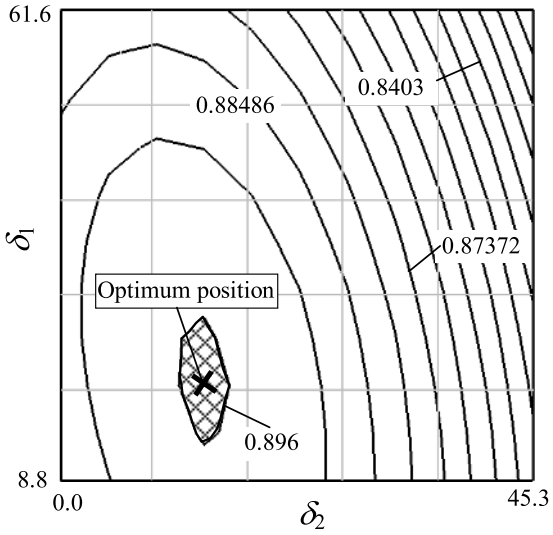

Fig. 8 Response surface (contour intervals = 0.005 57)

Table 4 Results of optimization

	Reference shape	Optimized shape	Increment %
Total pressure $P_o/P_{o\,ref}$	2.078	2.016	-2.98
Total temperature $T_o/T_{o\,ref}$	1.263	1.248	-1.19
Adiabatic efficiency %	88.46	89.57	1.25

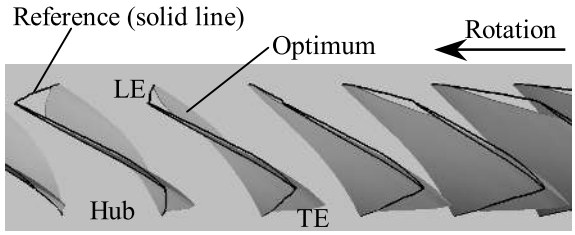

(a) View form casing

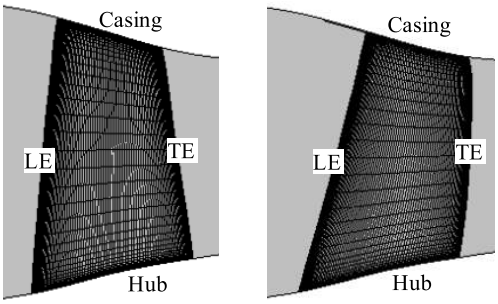

(b) Meridional view

Fig. 9 Blade shape

of the rotor affects substantially the adiabatic efficiency of the compressor rotor.

4.3 Flow characteristics of reference and optimized blades

The internal flow characteristics of the rotor have been analyzed to understand the effects of blade sweep on the efficiency. Figures 10 and 11 show Mach number and pressure contours on the plane of 40 percent span for the reference and the optimized blades, which are perspective view from the casing. The 40 percent span is the position where a relatively large increase in adiabatic efficiency is observed as shown in Fig. 6. In Fig. 10, the inflow is accelerated to supersonic state near the inlet of the blade passage. That is, a bow shock is generated upstream of the leading edge of the rotor, and a passage shock develops at the rotor suction surface. It is found that the interference position of the passage shock with the blade suction surface is moved downstream for the optimum blade compared to that for the reference one. On the other hand, the pressure recovery is relatively delayed throughout the blade passage in the optimum blade as shown in Fig. 11. Low pressure is observed at upstream of the passage shock where high Mach number is distributed.

Figures 12 and 13 show Mach number and pressure contours on the plane of 90 percent span for the reference and the optimized blades, which are shown in the same manner as in Figs. 10 and 11. The 90 percent span is the location where the optimum blade dose not show the improvement of efficiency as shown in Fig. 6. The pattern of a shock and its interference position with the blade suction surface are almost same for both the cases as shown in Fig. 12. Pressure recovery is also delayed along the blade passage in the optimum blade as shown in Fig. 13.

Figure 14 shows the pressure contours on the blade

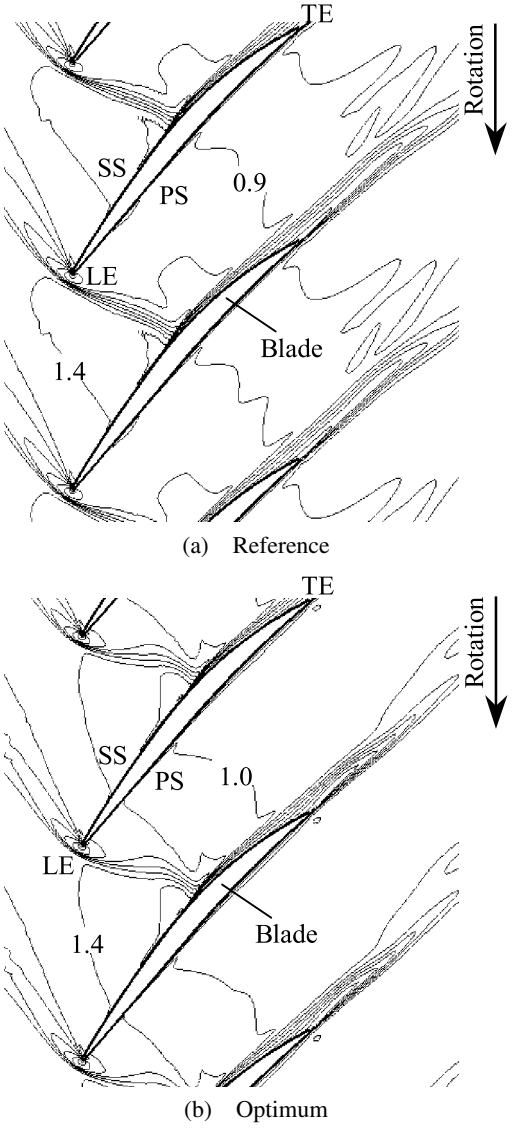

Fig. 10 Mach number contours on the plane of 40 percent span (interval of contour lines = 0.1)

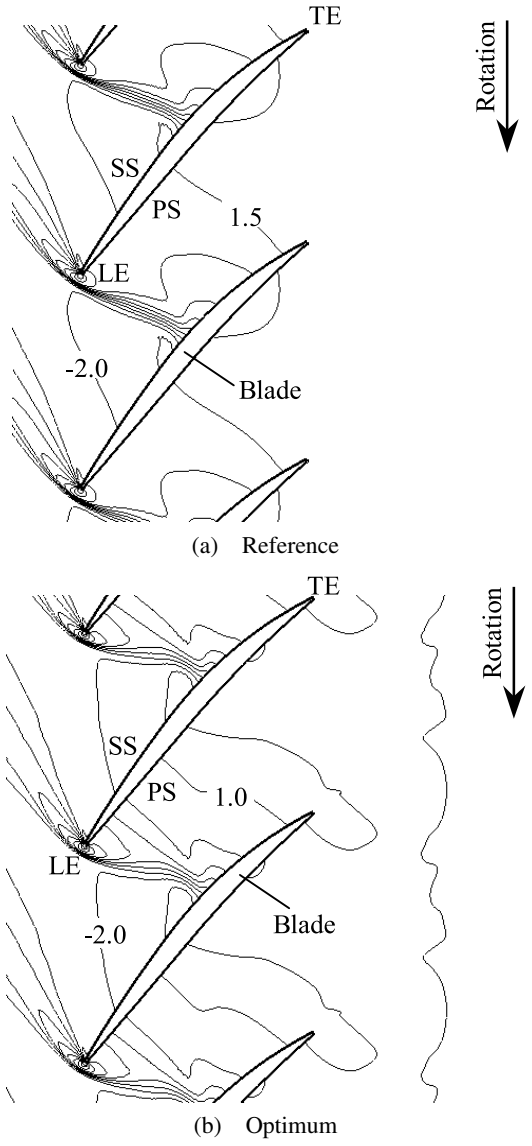

Fig. 11 Pressure contours on the plane of 40 percent span (interval of contour lines = 0.5)

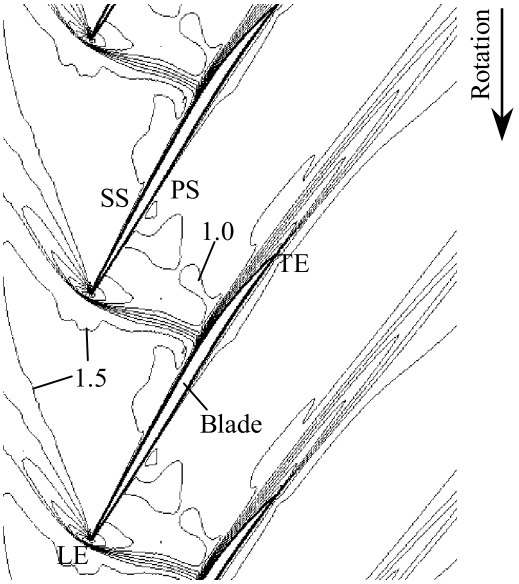

(a) Reference

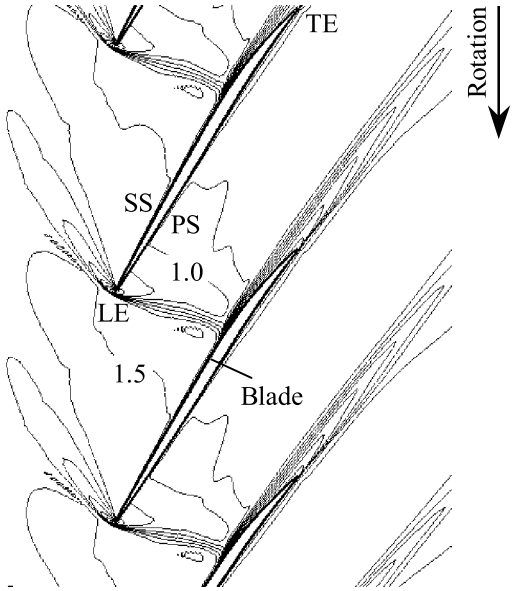

(b) Optimum

Fig. 12 Mach number contours on the plane of 90 percent span (interval of contour lines = 0.1)

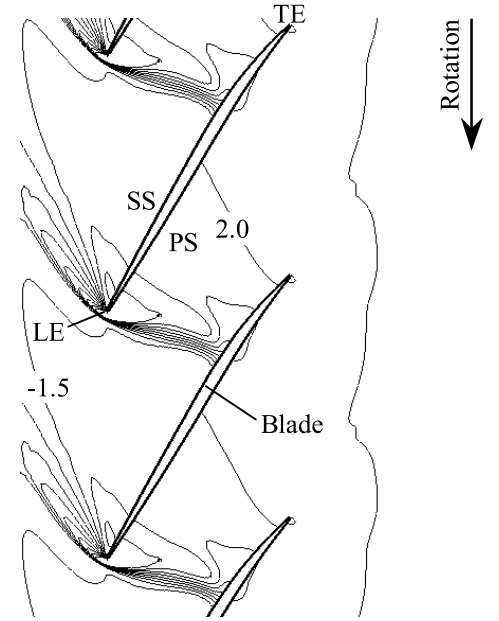

(a) Reference

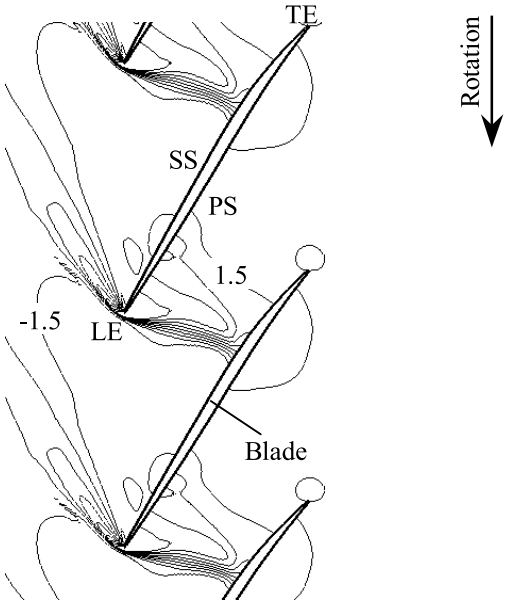

(b) Optimum

Fig. 13 Pressure contours on the plane of 90 percent span (interval of contour lines = 0.5)

suction surface for the reference and the optimized blades. In the figure, two solid lines indicate the positions of 40 and 90 percent spans. Generally, it is shown that the pressure recovery of the optimized blade is retarded as compared to that of the reference blade. The position of a shock on the blade suction surface, where the dense distribution of pressure is presented, is moved downstream near the mid-span for the optimized blade. At the 90 percent span, the position of a shock is located at 62.5 percent chord from the blade leading edge for both the cases. However, the position of a shock for the reference and optimized blades at the 40 percent span is observed at 51.5 and 57.8 percent chord from the leading edge, respectively. Therefore, it can be understood that the movement of the shock towards the downstream is effective in increasing the efficiency as shown in Fig. 6.

Figure 15 shows the limiting streamlines on the rotor suction surface for both the cases. Near the mid-chord of the blade passage, separation line is formed due to interference between the shock and the suction surface boundary layer in both the cases. An attachment line is observed behind the separation line for both the cases, which gives rise to separation bubble region between the separation and the attachment lines. It is noted that the flow pattern downstream of the separation line is more complex

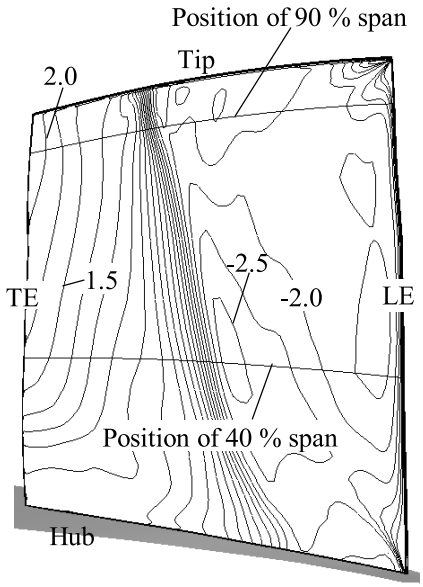

(a) Reference

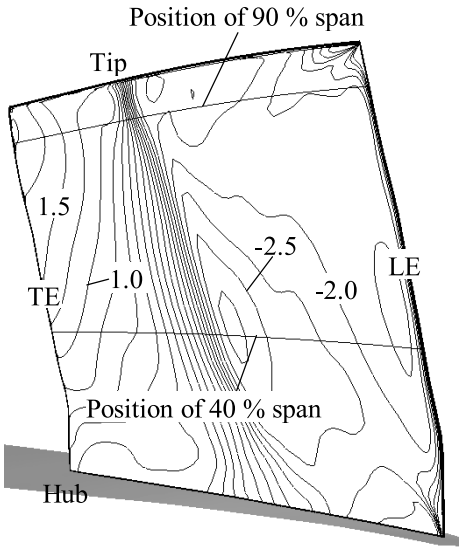

(b) Optimum

Fig. 14 Pressure contours on the blade suction surface

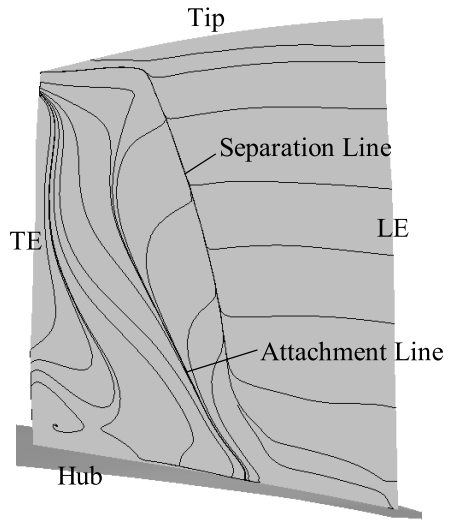

(a) Reference

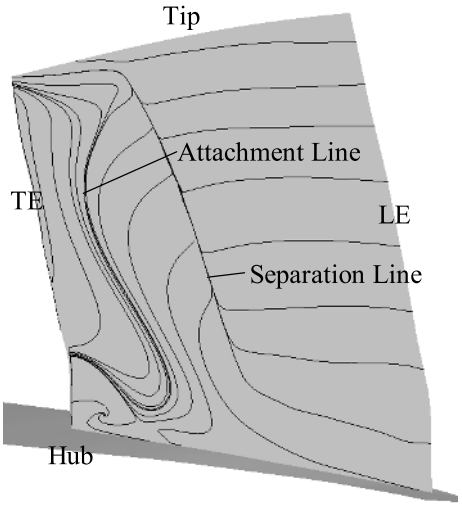

(b) Optimum

Fig. 15 Limiting streamlines on the blade suction surface

for the reference blade. The separation line is also moved downstream near the mid-span for the optimized blade as discussed in Fig. 14. It is well known that the separation on the blade suction surface deteriorates the performance of a turbomachinery. It should be noted that the increase in adiabatic efficiency for the optimized blade is caused by moving the separation line to the downstream on the blade suction surface.

5. Conclusion

The shape optimization of a rotor blade for transonic axial compressor was performed by the response surface method and the three-dimensional Navier-Stokes analysis. By optimizing the blade sweep of the rotor blade, the adiabatic efficiency is increased by 1.25 percent as compared to that of the reference shape. The response surface obtained with seven numerical experiments for two design variables is proved to be sufficiently reliable. It is found that the optimum shape improves the efficiency mainly in the middle of the span. The increase in adiabatic efficiency for the optimized blade is caused by moving the separation line to the downstream on the blade suction surface.

Acknowledgment

The authors would like to acknowledge the support from KISTI (Korea Institute of Science and Technology Information) under 'The Sixth Strategic Supercomputing Support Program.' The use of the computing system of the Supercomputing Center is also greatly appreciated.

References

(1) Suder, K.L. and Celestina, K.L., Experimental and Computational Investigation of the Tip Clearance Flow

in a Transonic Axial Compressor Rotor, ASME Paper 94-GT-365, (1994).
(2) Hah, C., Rabe, D.C. and Wadia A.R., Role of Tip Leakage Vortices and Passage Shock in Stall Inception in a Sweep Transonic Compressor Rotor, ASME GT2004-53867.
(3) Chima, R.V., Calculation of Tip Clearance Effects in a Transonic Compressor Rotor, ASME J. Turbomach., Vol.120, No.1 (1998), pp.131–140.
(4) Xu, C. and Amano, R.S., Numerical Prediction of Swept Blade Aerodynamic Effects, Proc. of ASME Turbo Expo 2004, ASME GT2004-53008.
(5) Bliss, D.B., Method and Apparatus for Preventing Leading Edge Shock Related Noise in Transonic and Supersonic Blades and Like, US Patent 3989406, (1976).
(6) Hah, C., Puterbaugh, S.L. and Wadia, A.R., Control of Shock Structure and Secondary Flow Field Inside Transonic Compressor Rotor through Aerodynamic Sweep, ASME 99-GT-561.
(7) Watanabe, H. and Zangeneh, M., Design of the Blade Geometry of Swept Transonic Fans by 3D Inverse Design, Proc. of ASME Turbo Expo, GT-2003-38770.
(8) Denton, J.D. and Xu, L., The Effects of Lean and Sweep on Transonic Fan Performance, Proc. of ASME Turbo Expo, GT-2002-30327.
(9) Vad, J., Kwedikha, A.R.A. and Jaberg, H., Influence of Blade Sweep on the Energetic Behavior of Axial Flow Turbomachinery Rotors at Design Flow Rate, Proc. of ASME Turbo Expo, GT-2004-53544.
(10) Myers, R.H. and Montgomery, D.C., Response Surface Methodology: Process and Product Optimization Using Designed Experiments, (1995), John Wiley & Sons.
(11) Ahn, C.S. and Kim, K.Y., Aerodynamic Design Optimization of a Compressor Rotor with Navier-Stokes Analysis, Proceedings of the Institution of Mechanical Engineers, Part A—Journal of Power and Energy, Vol.217, No.2 (2003), pp.179–184.
(12) Reid, L. and Moore, R.D., Design and Overall Performance of Four Highly-Loaded, High-Speed Inlet Stages for an Advanced, High-Pressure-Ratio Core Compressor, NASA TP-1337, (1978).
(13) Myers, R.H., Response Surface Methodology-Current Status and Future Direction, J. Quality Technology, Vol.31, No.1 (1999), pp.30–44.
(14) Box, M.J. and Draper, N.R., Fractional Designs, the $|X^TX|$ Criterion, and Some Related Matters, Technometrics, Vol.13, No.4 (1971), pp.731–742.
(15) Jameson, A., Schmidt, W. and Turkel, E., Numerical Solutions of the Euler Equation by Finite Volume Methods Using Runge-Kutta Time Stepping Schemes, AIAA Paper No.81-1259 (1981).
(16) Baldwin, B.S. and Lomax, H., Thin Layer Approximation and Algebraic Model for Separated Turbulent Flow, AIAA Paper No.78-257 (1978).
(17) Lee, S.Y. and Kim, K.Y., Design Optimization of Axial Flow Compressor Blades with Three-Dimensional Navier-Stokes Solver, KSME Int. J., Vol.14, No.9 (2000), pp.1005–1012.
(18) Guinta, A.A., Aircraft Multidisciplinary Design Optimization Using Design of Experimental Theory and Response Surface Modeling Methods, Ph.D. Dissertant, Department of Aerospace Engineering, Virginia Polytechnic Institute and State University, Blacksburg, VA., (1997).